CPP

Contributions to Plasma Physics

WILEY-VCH

REPRINT

Pressure-Driven Enthalpic and Lifshitz Transition in 122-Pnictides

K. F. Quader[1][*] and **M. Widom**[**][2]

[1] Department of Physics, Kent State University, Kent, OH 44242, USA
[2] Department of Physics, Carnegie-Mellon University, Pittsburgh, PA 15213, USA

Iron-arsenic pnictides are a class of compounds in which strong Coulomb interactions manifest in novel properties. We discuss basic ideas behind a Lifshitz transition and review salient properties of 122-pnictides ($A\mathrm{Fe}_2\mathrm{As}_2$; A = Ca, Sr, Ba, Ra). Using $T = 0$ first principles total energy calculations, as a function of hydrostatic pressure, we show that several pressure-driven anomalies, and the tetragonal (T) to collapsed tetragonal (cT) phase transition in the 122-pnictides family, can be understood as consequences of Lifshitz transitions arising from nontrivial changes in Fermi surface topology. We also show that several features found in our calculations, namely, enthalpic, magnetic and T-cT transitions, are universal to the 122-pnictides.

1 Introduction

Strong underlying Coulomb interactions manifest themselves in striking properties of highly correlated condensed matter systems. Recently discovered iron-arsenic pnictides are one class of these systems. A substantive amount of work dealing with these strong Coulomb interactions are rooted in total energy density functional methods, and another large body of research employs various many-particle techniques on renormalized shorter-range interactions to ascertain emergent collective behavior. These often complement each other.

In extended quantum condensed matter, lattice periodicity has to be taken into account in addition to Coulomb interactions. The Hamiltonian H is generally given by:

$$H = \frac{\hbar^2}{2m} \sum_i \nabla_i^2 - \sum_{i,I} \frac{Z_I e^2}{|r_i - R_I|} + \frac{1}{2} \sum_{i,j} \frac{e^2}{|r_i - r_j|} + \frac{\hbar^2}{2M} \sum_I \nabla_I^2 + \frac{1}{2} \sum_{i,J} \frac{Z_I Z_J e^2}{|R_I - R_J|} \qquad (1)$$

where the first three terms on the right hand side refer to the electronic part; the rest to the nucleons. m and M are respectively electron and nucleon mass, Z_I is the nucleon charge, r_i and R_I are the electron and nucleon positions respectively. In a solid, wherein normally the electronic part is dominant, obtaining ground and excited state properties entail treatment at the independent-particle level, and Coulomb repulsion and exchange correlations at the many-body level. Owing to underlying lattice structure, consideration of space group symmetries are useful.

Theory research on strongly coupled electrons in solids essentially fall into the following broad classes: Density functional theory (DFT) has been successful in determining zero temperature electronic structure and ground state, and can provide information on structural and magnetic phase transitions. Quantum Monte Carlo (QMC) simulations, based mostly on model interactions, attempt to obtain ground state properties; the fermion "minus-sign problem" however has to be dealt with. Several many-fermion perturbative techniques on renormalized or model Hamiltonians, such as Hubbard, Heisenberg, t-J models, have been employed to obtain ground state, collective excitations and emergent phenomena.

Our work here is based on $T = 0$ first principles total energy DFT calculations on 122-pnictides family (AFe2As2; A = alkali earth element Ca, Sr, Ba) as a function of hydrostatic pressure, We find that several pressure-driven anomalies, and the tetragonal (T) to collapsed tetragonal (cT) phase transition in the 122 family, can be understood as consequences of $T = 0$ Lifshitz transitions (LTs), arising from nontrivial changes in

---

[*] Corresponding author. E-mail: quader@kent.edu, Phone: +001 330 672 2915, Fax: +001 330 672 2959
[**] E-mail: widom@andrew.cmu.edu

Fermi surface topology. In addition, our results for band dispersions and spectra, lattice parameters, enthalpies, magnetism, and elastic constants over a wide range of pressure demonstrate that multiple transitions, namely, enthalpic, magnetic and T-cT transitions, are universal to the 122-pnictides.

1.1 Lifshitz Transition

Lifshitz transitions (LTs) [1], topological changes of a material's Fermi surface caused by external pressure or chemical substitution, are of considerable current interest. As shown in Fig. 1, changes in electronic band structure, such as disruption or creation of a Fermi surface neck, and creation or disappearance of a pocket, constitute typical topological changes; see Fig. 1. Because they require band dispersion extrema, LTs often appear on points or lines of high symmetry in the Brillouin zone. They are generally correlated with a van Hove singularity crossing the Fermi level, though this may not be straightforward to ascertain in non-elemental systems with complicated densities of states. At $T = 0$, LTs are true phase transitions of order 2 1/2, as in Ehrenfest's classification. This can be understood by considering in 3D a change in thermodynamic potential, $\delta\Omega \propto |\epsilon_F - \epsilon_c|^{5/2} \equiv |z|^{5/2}$, where z is the distance from the quantum critical point, ϵ_c, and Ω the thermodynamic potential. Then both Ω, $\delta\Omega/\delta\epsilon_F$ are differentiable; $\delta^2\Omega/\delta^2\epsilon_F$ is continuous, but possess a vertical kink, and hence not differentiable; and $\delta^3\Omega/\delta^3\epsilon_F$ is infinite. At finite T, thermal smearing of the Fermi surface causes rapidly varying but analytic crossovers of properties [2]. Resulting anomalies in lattice parameters, density of states near the Fermi energy E_F, elastic properties, and electron dynamics manifest in observable thermodynamic and transport properties [1, 2]. Present-day angle resolved photoemission spectroscopy (ARPES) experiments are capable of mapping Fermi surface topology, and thus can provide a more direct signature of LTs.
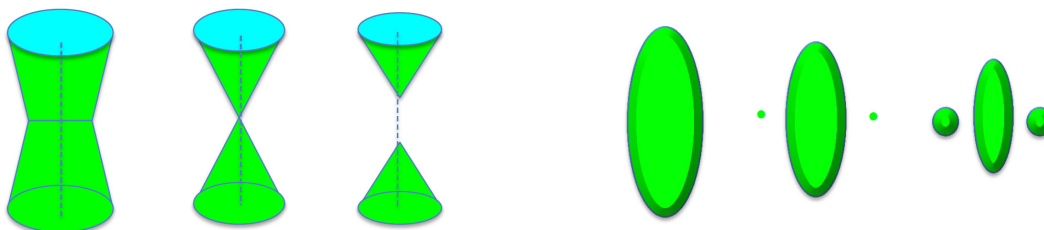
Fig. 1 Changes in band structure that may lead to Lifshitz transition. (Left): Disruption or creation of a Fermi surface neck; (Right): Creation or disappearance of a Fermi surface pocket.

In the past, theoretical evidence for LTs under pressure have been found, for example, in DFT calculations of Zn and Cd [3], and Os [4]. Effects of LTs on thermodynamic and transport properties may be small and hence pose challenges for experimentalists. Nevertheless, LTs have been deduced, for example, from pressure study of elastic constants in YCo$_5$ [5], Shubnikov-dHvA effect in Cd [6], and through the superconducting transition temperature (T$_c$) and magnetothermopower in Al [7]. Of late, there has been interest in exploring possible effects of LTs in the iron arsenic compounds. While at present there are no claims of observation of LTs in the pnictides under external pressure, recent ARPES experiments and theoretical interpretation provide evidence for LTs in doped Ba-122 [8, 9], and interesting changes in electronic structure in Ca-122 [10] subjected to internal strain.

1.2 Features of 122-pnictides

The 122 pnictides, AFe$_2$As$_2$ (A = Ca, Sr, Ba), display structural, magnetic or superconducting phase transitions upon doping or applied pressure [11–14]; notably, a tetragonal phase (T) with a large c-axis, "collapses" to a phase (cT) with a smaller c-axis. Both tetragonal phases share the space group I4/mmm. We include in our results, A = Ra, as it clarifies trends in behavior of the 122 series.

The 122 pnictides share common structures (Fig. 2). At ambient pressure, Ca-, Sr-, Ba-122 compounds exhibit transitions from the high-temperature tetragonal (T) phase to a low temperature orthorhombic (OR) phase (space group Fmmm), striped along the a-axis and antiferromagnetically (AFM) ordered along the c-axis, at T$_{OR}$ ∼ 170 K, 205 K, 140 K respectively [15–17]. This may be viewed as a magneto-structural transition from a high-T phase

with fluctuating magnetic moments [18] to one with long-range AFM order. The T-OR transition temperature T_{OR} decreases with applied pressure.

Under hydrostatic pressure, at low-T, the 122-pnictides lose their OR-AFM state. Ca-122 and Sr-122 exhibit 1st-order transitions to the collapsed tetragonal (cT) phase with decreased c-axis value, at $P \sim 0.35$ GPa [19], and uncollapsed tetragonal (T) phase at $P \sim 4.4$ GPa [20, 21] respectively. Ba-122 appears to undergo a continuous (or weakly 1st-order) transition at $P \sim 10.5$ GPa [22–24] to a T phase; experiments are variously at T $\sim$ 33K and 100K. The critical pressures tend to be lower under non-hydrostatic conditions. With increased pressure, the T phase a- and c-axis parameters decrease smoothly until pressures, $P \sim 7$-10 GPa [20, 25, 26] and 29 GPa [22, 27] respectively for Sr-122 and Ba-122, at which they evolve anomalously until the cT state is reached. High pressure x-ray diffraction studies of the Ba-122 and Sr-122 compounds attributed [26, 27] these lattice parameter anomalies to a negative compressibility along the a-axis.
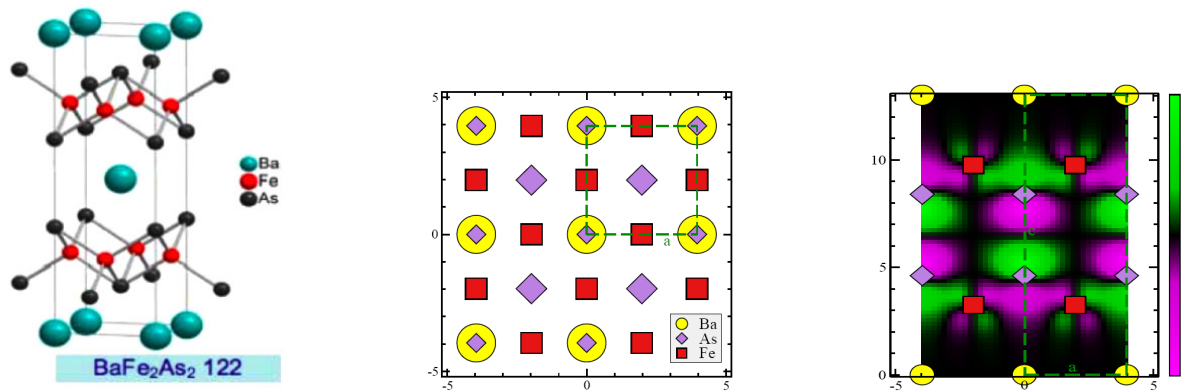
Fig. 2 (Right): Lattice Structure of Ba-122 pnictide. All 122 pnictides $A\mathrm{Fe_2As_2}$ (A = Ca, Sr, Ba) possess this structure. (Center): Structure of Ba-122 tetragonal (T) phase viewed along the (001) axis, from $z = 0$ to $c/2$. xy coordinates are given in units of Å. Atom size indicates z position, with large below small. (Right): Structure within the xz-plane at $y = 0$. Atoms are color-coded as on left. Background illustrates a purely real X-point wavefunction (see text), with scale bar linear in value.

2 Method

Our DFT total energy study systematically explores the different pressure-driven transitions in the entire alkaline earth 122-pnictide family. To explore dependence on the alkaline earth element A, in addition to Ca-, Sr- and Ba-122 pnictides, we also performed DFT calculations on $\mathrm{RaFe_2As_2}$ and $\mathrm{MgFe_2As_2}$ and compared their enthalpies to the pure elements and known stable binary phases. $\mathrm{MgFe_2As_2}$ is found to be energetically unfavorable, both in its tI10 and oF20 forms. However, we predict that $\mathrm{RaFe_2As_2}$, which may not be feasible to synthesize, is stable, and its pressure-driven transitions closely resemble those of Ba-122.

Previous DFT calculations [28–30] have considered pressure and doping dependences. For Ba-122 two pressure-driven transitions were obtained, and abrupt jumps in the bulk modulus reported [29] at both low and high pressure transitions. A DFT-based molecular dynamics calculation [31] obtained two pressure-driven transitions in Ba-122 at low-T. At higher T, the sharp OR-T transition at $P \sim 12.5$ GPa is shifted up to 15 GPa, and somewhat smoothed out, and at higher pressure the T-cT transition becomes almost indiscernible.

2.1 DFT in a Nutshell and VASP Calculations

For bulk matter, atoms may be separated into positively charged, but relatively massive nuclei, so that they can be considered as fixed point charges, and negatively charged smaller mass electrons, that need to be described through a position-dependent many-body wave function that is the eigenvector of the Hamiltonian (Eq. 1). As can be seen there, electron-electron and electron-nuclei interactions are Coulombic. Owing to the high dimensionality of the Hilbert space involved, the many-body problem is computationally intractable without further approximations.

In Hohenberg-Kohn's [32] epic DFT formulation, the many-body problem is replaced by the much simpler problem of finding the central scalar quantity, the electron density $\rho(\mathbf{r})$, that minimizes the total energy functional $E[\rho(\mathbf{r})]$. Kohn-Sham [33] mapped this interacting many-body problem into auxiliary independent-particle equations, with many-body correlations and exchange effects encoded in an exchange-correlation functional, $V_{xc}[\rho(\mathbf{r})]$:

$$\left(-\frac{\hbar^2}{2m}\nabla_{\mathbf{r}}^2 + \int dr' \frac{\rho(\mathbf{r}')}{|\mathbf{r}-\mathbf{r}'|} + V_{xc}[\rho(\mathbf{r})]\right)\psi_i(\mathbf{r}) = \epsilon_{\mathbf{i}}\psi_{\mathbf{i}}(\mathbf{r}). \tag{2}$$

The equations for single-particle wavefunctions ψ_i are coupled through the electron density $\rho(\mathbf{r}) = \sum_{\mathbf{i=1}}^{\mathbf{N}} |\psi_{\mathbf{i}}(\mathbf{r})|^{\mathbf{2}}$. The challenge of DFT is to determine the best exchange-correlation functional for the system on hand; two commonly used are the local density approximation (LDA) and generalized gradient approximation (GGA). LDA replaces the exchange correlation functional with the value of the exchange correlation potential of a uniform electron gas whose density matches the local value of $\rho(\mathbf{r})$. GGA supplements LDA with corrections dependent on the gradient of the density at the same point.

Periodicity of a solid and the invariance of the Hamiltonian under point group symmetry operations imply that calculations need only be performed in a single unit cell, and so, momentum space ($\mathbf{k}$) points only in the irreducible Brillouin zone need to be considered.

Our calculation utilizes the plane-wave based DFT code, Vienna Ab-initio Simulation Package (VASP) [32] with the all-electron projector augmented wave method [33] carried out in the Perdew-Burke-Ernzerhof generalized gradient approximation [34] to the exchange-correlation potential.

We adopt the Pearson notation for crystal structures; this consists of: a *lowercase* letter a,m,o,t,h,c indicating, respectively asymmetric, monoclinic, orthorhombic, tetragonal, hexagonal and cubic; an *uppercase* letter PRFICBA indicating primitive, rhombohedral or some type of centering; a number indicating the number of atomic sites per unit cell. For example, hP2 indicates HCP, while cI2 indicates BCC. Here, our calculations are performed within the unit cells with Pearson type tI10 for the tetragonal phase and oF20 for the orthorhombic phase. However, a $\sqrt{2} \times \sqrt{2}$ supercell of tI10 is employed for consistency with oF20 for calculations of ΔH. Striped antiferromagnetic collinear spin configurations are utilized in the OR-AFM state.

Energy cutoffs and k-point meshes are increased to converge total energies to better than 1 meV/atom. In particular, we utilized a plane wave energy cutoff of 320 eV for all calculations reported, which exceeds the default cutoff for Fe by 20%. We employed k-point meshes ranging from $8 \times 8 \times 4$ for oF20 unit cells up to $11 \times 11 \times 5$ for tI10 unit cells and $11 \times 11 \times 11$ for tI10 primitive cells. Special k-points utilized in band structures are [35]: $\Gamma = (0,0,0)$, $X = (0,0,1/2)$, $M = Z' = (-1/2, 1/2, 1/2)$, and $Z = (1/2, 1/2, -1/2)$ in reciprocal coordinates. All calculations were performed using the VASP setting PREC=Accurate so as to avoid Fourier transform wrap-around errors. Fermi surface smearing of 0.2 eV is employed for relaxations and 0.05 eV for ΔH values. Precise transition pressures were found to be sensitive to smearing, but we did not attempt to converge in this variable. Densities of states utilize tetrahedron integration with subsequent Gaussian smearing of 0.01 eV. Elastic constants were calculated within VASP by finite differences of stress with respect to strain.

To observe pressure-driven transitions we begin with $P = 0$ structures and increase the pressure in steps of 1 GPa (0.5 GPa for the case of Ca-122), fully relaxing the lattice parameters and internal coordinates at each step until the maximum force is less than 0.01 eV/Å. Accurate values for P_H and P_L were obtained by linear interpolation to locate $\Delta H = 0$ (for P_H) and $E(k) = E_F$ (for P_L), while steps as low as 0.1 GPa were utilized to resolve P_M.

3 Calculated Transitions Under Pressure

Our key results are summarized in Fig. 3. We find three types of transition to occur: an enthalpic transition, in which the OR-AFM state loses thermodynamic stability to a tetragonal state; a magnetic transition, in which the OR-AFM state loses its magnetic moment; a transition in which the tetragonal T state collapses to cT, identified as the Lifshitz transition; see Section 4. These transitions occur in different sequences depending on A; hence some occur within metastable states and will not be observed in experiments in thermodynamic equilibrium.

Enthalpic transition at P_H: This is shown in Fig. 3a. For A=Ca, both OR-AFM and nonmagnetic states exist simultaneously at pressures above and below P_H. However, high-P favors the lower volume cT state causing the enthalpy difference $\Delta H \equiv H_{cT} - H_{OR} = \Delta E - P\Delta V$ to change sign at P_H [36]. The situation is similar for A=Sr, Ba, Ra, with the exception that the transition from OR-AFM is to an *uncollapsed* tetragonal state T, rather than the collapsed cT. For all A, the OR-AFM state continues as a metastable state for $P > P_H$ and no magnetic or lattice anomalies occur upon crossing P_H. P_H is progressively larger for A= Ca, Sr, Ba, Ra because ΔE is greater, and the volume difference ΔV is smaller. Because ΔH crosses zero linearly at P_H, these transitions are *first order* for all four 122 pnictides considered here, although in the case of Ba and Ra the transition is nearly continuous (i.e. weakly first order).
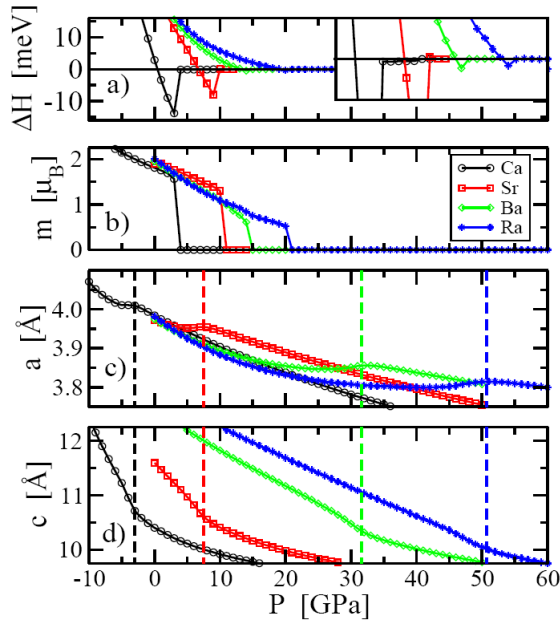
Fig. 3 Key pressure-dependent results for A-122 pnictides, A=Ca, Sr, Ba and Ra. a) Enthalpy differences $\Delta H = H_{cT} - H_{OR}$ between tetragonal and OR-AFM phases; the inset enlarges the $\Delta H = 0$ crossings. b) Magnetic moments vanishing abruptly at the magnetic transition P_M. c) and d) show the anomalous behavior of the tetragonal a and c axis parameters. Vertical dashed lines indicate T - cT transition (identified as the Lifshitz transition) pressures, P_L.

Magnetic transition at P_M: For all four 122 compounds, the magnetic moments vanish suddenly, i.e. no stable OR-AFM state exists for $P > P_M$, even though it exists and maintains a large magnetic moment for $P_H < P < P_M$; see Fig. 3b. Note the strict inequality $P_H < P_M$ owing to the metastable (*i.e.* mechanically stable but enthalpically unfavorable) extension of the OR-AFM state, a distinction not widely recognized. [29,30] Thus for Ca-122 and Ba-122, P_c and P_{c1} respectively [29] correspond to our P_M; not distinguishing this from P_H can lead to a large error in estimating the critical pressure for Ca-122. Distinguishing P_H from P_M allows us to recognize that though a striped-AFM state exists for $P_H < P < P_M$, it is not stable for $P > P_M$, in contrast with previous work [30]. The existence of the metastable state is verified by the experimental observation of hysterisis in the case of Ca-122 [37].

Collapsed Tetragonal Phase - Characteristic Pressure P_L: In our picture, P_L separates the two tetragonal states, T and cT. Fig. 3c,d) shows that for all four 122-pnictides, P_L is characterized by anomalies in tetragonal a and c axis lattice parameters. The a axis varies non-monotonically, and c-axis shows an inflection, although the unit cell volume $V = a^2 c$ decreases monotonically with P as required by thermodynamics. P_L increases monotonically with A as it advances down the periodic table. For A=Ca, we find the anomalies in a and c occur at a negative pressure, P_L = -3.2 GPa, and hence the transition at P_H = 0.46 GPa goes directly from OR to cT. The transitions are fully reversible, as the lattice parameter curves exactly reproduce without hysteresis under increasing or decreasing pressure.

4   T - cT Transition driven by Lifshitz Transition

We have discussed in Sec. 3C that, for each of the 122-pnictides, a characteristic pressure, P_L can be associated with the anomalous behavior in the tetragonal a and c lattice parameters, and the T - cT transition; see Fig. 3c,d).

Below, we show that our calculations of electronic structure, elastic constants, and bond lengths, for different pressures, in the 122-pnictides, provide support to our claim that the T - cT transition arises from a Lifshitz transition.

Electronic Structure: Our electronic structure calculations give *band dispersions* along different k-directions, and also the density of states (DOS) integrated over the full Brillouin zone. Since the results are similar overall for all 122-pnictides, as a prototypical case, we discuss in details the Ba-122 compound.
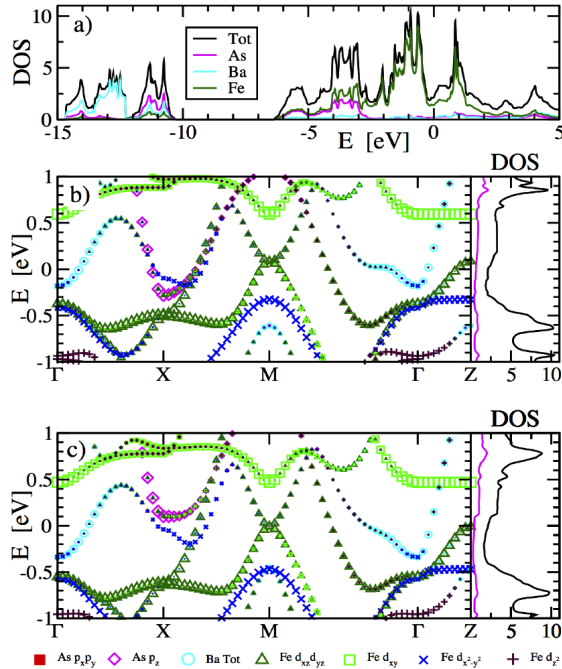
Fig. 4 Band structure and density of states (DOS) for Ba-122 a) Total density of states (DOS) and Fe, As, and Ba partial DOS over a wide range of energy at $P = 28$ GPa. b) and c) Band structures in the primitive tetragonal cell Brillouin zone [29,35] at $P = 28$ and $P = 34$ GPa, i.e., below and above P_L respectively. The corresponding total and As partial DOS around E_F are shown alongside; the As DOS has been scaled 3x to make it more visible. Note that the As p_z electron pocket at the X point moves above E_F for $P > P_L$. Plotting symbol size indicates the projection onto atomic orbitals.

Fig. 4 shows the dispersion relations for individual bands for Ba-122 at representative pressures. We draw particular attention to the band at the X-point, comprised mostly of anti-bonding As-p_z, mixed with bonding Fe-$d_{xz,yz}$ orbitals (see wavefunction in Fig. 2). As Fig. 4b) shows, this band lies below E_F at $P = 28$ GPa, forming an electron pocket, while Fig. 4c) shows that at $P = 34$ GPa, this band has moved to above E_F, so that the electron pocket has emptied; the transition occurs at $P_L = 31.6$ GPa.

Pressure dependence of this and other bands are illustrated Fig. 5a,b). This topological change in the Fermi surface correlates strongly with the anomalous behavior of the a and c lattice parameters discussed above and shown in Fig. 3. We take this X-point band crossing to define the value of P_L, which we recognize as a Lifshitz transition. This corresponds to a van Hove singularity in DOS that moves across E_F, and can be seen most clearly above P_L in Fig. 4c). Additional bands can be seen crossing E_F in Fig. 5a,b) indicating that other Lifshitz transitions exist, which is not surprising given the large number of bands in a crystal structure with many atoms per unit cell.

Elastic Constants and Bond Lengths: Fig. 5c) shows the variation of the calculated tetragonal elastic constants with pressure. While most elastic constants increase monotonically with pressure, C_{33}, related to stress-strain along the c-axis, displays anomalous behavior around the T-cT Lifshitz transition pressure, P_L. Slightly below P_L, C_{33} decreases with pressure to a minimum, and then increases again beyond P_L. As can be seen, C_{33} lies above the limit of elastic stability [38], i.e. $C_{33} > C^* = 2C_{13}^2/(C_{11} + C_{12}) = 86$ GPa, given the values of C_{ij} at P_L. Evidently, the T phase is heading towards an elastic instability in the vicinity of P_L that is avoided by the transition into the cT state. We note that C_{33}, and hence compressibility, does not go negative, contrary to some views in literature [26, 27].

Fig. 5d) shows the behavior of various calculated bond-lengths with pressure. The As-As bond length drops below 3 Å, reaching 2.9 Å as $P \rightarrow P_L$. As we discussed above, the X-point band that crosses E_F at P_L is

dominated by As-p_z orbitals between As atoms that are neighbors in the z-direction, and hence their separation closely tracks the variation of the c axis. As the As-As bond length drops, causing the energy of this repulsive anti-bond (shown in Fig. 2b) to rise towards E_F, the resulting depletion of the repulsive bond softens C_{33}. Following the collapse, other repulsive forces stabilize the structure with a reduced c-axis, as can be seen in the subsequent rise of C_{33}. The same wavefunction is bonding between As and Fe (Fig. 2b), so its depletion can be associated with the increase in the a lattice parameter. Presumably the value of P_L grows with increasing atomic radius of the alkali earth element because greater pressure is required to drive the As-As bond length below 3 Å.
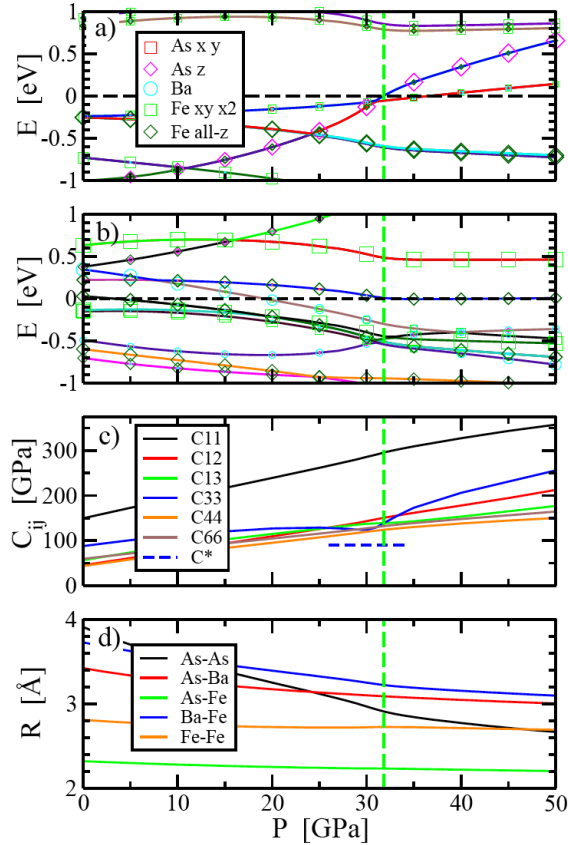
Fig. 5 Pressure variations of key quantities for Ba-122. a) X-point bands; b) M- and Γ-point bands. Dashed vertical line locates P_L. c) Tetragonal elastic constants calculated within VASP. The dashed horizontal line indicates the limit for elastic stability (see text). d) Interatomic separations.

5 Discussion

Our calculations show that the alkaline earth 122 pnictides, under pressure, exhibit several features which are universal within this family. One key result is that at high pressures these pnictides exhibit Lifshitz transitions characterized by the vanishing of an electron pocket at the X-point, as it moves from below to above the Fermi energy. This correlates well with anomalies in lattice parameters and elastic constants around the Lifshitz transition pressure, P_L. We suggest that the finite-temperature T-cT transitions, that occur in all the 122 compounds, are consequences of the $T = 0$ Lifshitz transitions. This provides a novel explanation for the observed anomalies in lattice parameters and elastic constants, and one that is different from those existent in literature. At finite-T, the Lifshitz transition normally becomes a smooth crossover, but could conceivably be driven first order through lattice phonons and/or spin fluctuations. At lower pressures, P_H, these 122-pnictides all undergo first-order enthalpic transitions from a AFM-OR phases to non-magnetic T or a cT phases. In all cases, metastable magnetic OR phases persist up to higher pressures, P_M when magnetism is lost by first-order transitions.

References

[1] I. M. Lifshitz, Sov. Phys. JETP **11**, 1130 (1960).

[2] A. Varlamov, V. Edorov, and A. Pantsulaya, Advances in Physics **38**, 469 (1989).

[3] D.L. Novikov, M.I. Katsnelson, A.V. Trefilov, A.J. Freeman, N.E. Christensen, A. Svane, and C.O. Rodriguez, Phys. Rev. B **59**, 4557 (1999).

[4] D. Koudela, M. Richter, A. Möbius, K. Koepernik, and H. Eschrig, Phys. Rev. B **74**, 214103 (2006).

[5] H. Rosner, D. Koudela, U. Schwarz, A. Handstein, M. Hanfland, I. Opahle, K. Koepernik, M.D. Kuz'min, K.H. Muller, J.A. Mydosh, and Richter, Nat Phys **2**, 469 (2006).

[6] S.L. Bud'ko, A.N. Voronovskii, A.G. Gapotchenko, and E.S. ltskevich, Zh. Eksp. Teor. Fiz. **86**, 778 (1984).

[7] D.R. Overcash, T. Davis, J.W. Cook, and M.J. Skove, Phys. Rev. Lett. **46**, 287 (1981).

[8] C. Liu, T. Kondo, R.M. Fernandes, A.D. Palczewski, E.D. Mun, N.A. Ni, A.N. Thaler, A. Bostwick, E. Rotenberg, J. Schmalian, S.L. Bud'ko, P.C. Canfield, and A. Kaminski, Nat Phys **6**, 419 (2010).

[9] C. Liu, A.D. Palczewski, R.S. Dhaka, T. Kondo, R.M. Fernandes, E.D. Mun, H. Hodovanets, A.N. Thaler, J. Schmalian, S.L. Bud'ko, P.C. Canfield, and A. Kaminski, Phys. Rev. B **84**, 020509 (2011).

[10] R. Dhaka, R. Jiang, S. Ran, S. Bud'ko, P. Canfield, M. Tomi'c, R. Valent'i, Y. Lee, B. Harmon, and A. Kaminski, arXiv:1401.5461 (2014).

[11] P. Alireza, Y.T. Ko, J. Gillett, C.M. Petrone, J.M. Cole, G.G. Lonzarich, and S.E. Sebastian, J. Phys. : Condens. Matter **21**, 012208 (2009).

[12] M.S. Torikachvili, S.L. Bud'ko, N. Ni, P.C. Canfield, and S.T. Hannahs, Phys. Rev. B **80**, 014521 (2009).

[13] A. Mani, S. Ghost, S. Paulraj, A. Bharathi, and C.S. Sundar, Europhys. Lett. **87**, 17004 (2009).

[14] S.R. Saha, N.P. Butch, T. Drye, J. Magill, S. Ziemak, K. Kirshenbaum, P.Y. Zavalij, J.W. Lynn, and J. Paglione, Phys. Rev. B **85**, 024525 (2012).

[15] M.S. Torikachvili, S.L. Bud'ko, N. Ni, and P.C. Canfield, Phys. Rev. B **78**, 104527 (2008).

[16] C. Krellner, N. Caroca-Canales, A. Jesche, H. Rosner, A. Ormeci, and C. Geibel, Phys. Rev. B **78**, 100504 (2008).

[17] Q. Huang, Y. Qiu, W. Bao, M.A. Green, J.W. Lynn, Y.C. Gasparovic, T. Wu, G. Wu, and X.H. Chen, Phys. Rev. Lett. **101**, 257003 (2008).

[18] S.O. Diallo, D.K. Pratt, R.M. Fernandes, W. Tian, J.L. Zarestky, M. Lumsden, T.G. Perring, C.L. Broholm, N. Ni, S.L. Bud'ko, P.C. Canfield, H.F. Li, D. Vaknin, A. Kreyssig, A.I. Goldman, and R.J. McQueeney, Phys. Rev. B **81**, 214407 (2010).

[19] P. Canfield, S. Budko, N. Ni, A. Kreyssig, A. Goldman, R. McQueeney, M. Torikachvili, D. Argyriou, G. Luke, and W. Yu, Physica C **469**, 404 (2009).

[20] S. Ikeda, K. Yoshida, and H. Kobayashi, Hyperfine Interactions **208**, 7 (2012).

[21] H. Kotegawa, T. Kawazoe, H. Sugawara, K. Murata, and H. Tou, J. Phys. Soc. Jpn **78**, 083702 (2009).

[22] R. Mittal, S.K. Mishra, S.L. Chaplot, S.V. Ovsyannikov, E. Greenberg, D.M. Trots, L. Dubrovinsky, Y. Su, T. Brueckel, S. Matsuishi, H. Hosono, and G. Garbarino, Phys. Rev. B **83**, 054503 (2011).

[23] W.J. Duncan, O.P. Welzel, C. Harrison, X.F. Wang, X.H. Chen, F.M. Grosche, and P.G. Niklowitz, Journal of Physics: Condensed Matter **22**, 052201 (2010).

[24] T. Yamazaki, N. Takeshita, R. Kobayashi, H. Fukazawa, Y. Kohori, K. Kihou, C.H. Lee, H. Kito, A. Iyo, and H. Eisaki, Phys. Rev. B **81**, 224511 (2010).

[25] D. Kasinathan, M. Schmitt, K. Koepernik, A. Ormeci, K. Meier, U. Schwarz, M. Hanfland, C. Geibel, Y. Grin, A. Leithe-Jasper, and H. Rosner, Phys. Rev. B **84**, 054509 (2011).

[26] W.O. Uhoya, J.M. Montgomery, G.M. Tsoi, Y.K. Vohra, M.A. McGuire, A.S. Sefat, B. C. Sales, and S.T. Weir, Journal of Physics: Condensed Matter **23**, 122201 (2011).

[27] W. Uhoya, A. Stemshorn, G. Tsoi, Y.K. Vohra, A.S. Sefat, B.C. Sales, K.M. Hope, and S.T. Weir, Phys. Rev. B **82**, 144118 (2010).

[28] M.D. Johannes, I.I. Mazin, and D.S. Parker, Phys. Rev. B **82**, 024527 (2010).

[29] M. Tomic, R. Valenti, and H.O. Jeschke, Phys. Rev. B **85**, 094105 (2012).

[30] N. Colonna, G. Profeta, A. Continenza, and S. Massidda, Phys. Rev. B **83**, 094529 (2011).

[31] S. Backes and H.O. Jeschke, Phys. Rev. B **88**, 075111 (2013).

[32] P. Hohenberg and W. Kohn, Phys. Rev. B **136**, 864 (1964).

[33] W. Kohn and L.J. Sham, Phys. Rev. B **140**, 1133 (1965).

[34] J.P. Perdew, K. Burke, and M. Ernzerhof, Phys. Rev. Lett. **77**, 3865 (1996).

[35] O.K. Andersen and L. Boeri, Ann. Phys. **523**, 8 (2011).

[36] M. Widom and K. Quader, Phys. Rev. B **88**, 045117 (2013).

[37] A.I. Goldman, A. Kreyssig, K. Prokeš, D.K. Pratt, D.N. Argyriou, J.W. Lynn, S. Nandi, S. A. J. Kimber, Y. Chen, Y.B. Lee, G. Samolyuk, J.B. Leáo, S.J. Poulton, S.L. Bud'ko, N. Ni, P.C. Canfield, B.N. Harmon, and R. J. Mc- Queeney, Phys. Rev. B **79**, 024513 (2009).

[38] C. Kittel, Introduction to Solid State Physics, eighth edition (Wiley, 2005).